


Experimental Validation of a Multidimensional Model for an Indirect Temperature Swing Adsorption Unit

Thomas Ried^{1,2,*}, Gabriel Salazar Duarte¹, and Olaf Hinrichsen^{2,3}

DOI: 10.1002/cite.201900170

 This is an open access article under the terms of the Creative Commons Attribution-NonCommercial-NoDerivs License, which permits use and distribution in any medium, provided the original work is properly cited, the use is non-commercial and no modifications or adaptations are made.



Supporting Information
available online

Conventional temperature swing adsorption (TSA) is mainly applied for the removal of trace contaminants. Indirectly heated and cooled adsorbers were developed to make bulk separation economically feasible. A quasi-continuous TSA process to remove CO₂ from an N₂/CO₂ mixture with a pilot plant is established. The experimentally determined data are taken to validate and to adjust a 2D simulation model. For the validation, the CO₂ desorption, the N₂ recovery rate as well as the axial temperature profile are compared. The successful model validation can be seen in the good agreement between simulation and experimental results. Moreover, this process is able to separate high amounts of CO₂ and to produce a nearly CO₂-free product stream.

Keywords: Adsorption, CO₂ removal, Indirect heat transfer, Temperature swing adsorption

Received: October 23, 2019; *accepted:* March 30, 2020

1 Introduction

Adsorption processes are used to separate and to purify gas streams. A typical classification of adsorption processes is by their method of regeneration [1–3]. Most frequently applied processes are temperature swing adsorption (TSA) and pressure swing adsorption (PSA). The process selection depends on the boundary conditions and especially on the type and concentration of the compound(s) to be separated [2]. This work focuses on gas separation by a TSA process.

TSA is generally applied for purification and separation of strongly adsorbed compounds like H₂O or CO₂. In conventional TSA processes, the adsorber is heated and cooled directly with a regeneration gas. The regeneration gas can be a purified product, N₂ or any other suitable purge gas stream. [4, 5]

Adsorption is a batch process, so at least two adsorbers are necessary to establish a quasi-continuous process; one adsorber is in the adsorption step while the other runs through the regeneration phase. As the amount of regeneration gas is usually limited, the duration of the heating and cooling step is long. The duration is extended by the comparatively low heat capacity of the regeneration gas in combination with the low thermal conductivity of conventional adsorbent materials. Hence, the typical cycle time of a TSA is between hours and days. In relation to the concentration of the adsorbed compounds, large volumes of adsorbent are

necessary to ensure the required product purity throughout the whole cycle. [3]

Moreover, the heat of adsorption released during the adsorption step increases the temperature of the adsorbent bed and, therefore, reduces the adsorption capacity. As a result, a conventional TSA process is economically limited to the removal of trace impurities or contaminant gas concentrations in the lower percentage range. [5]

Different alternative concepts have been developed to reduce the heating and/or cooling time. Two main different approaches can be distinguished: electrothermal swing adsorption processes (ESA) [6] and indirectly heated and cooled TSA processes [7]. In an ESA process, the adsorbent is indirectly heated by energizing the solid adsorbent. For this separation, an electric conductive adsorbent material is required. An additional drawback of the ESA concept is that

¹Thomas Ried, Dr.-Ing. Gabriel Salazar Duarte
Thomas.ried@linde.com

Linde Aktiengesellschaft, Linde Engineering, Dr.-Carl-von-Linde-Straße 6–14, 82049 Pullach, Germany.

²Thomas Ried, Prof. Dr.-Ing. Olaf Hinrichsen
Technical University of Munich, Department of Chemistry,
Lichtenbergstraße 4, 85748 Garching, Germany.

³Prof. Dr.-Ing. Olaf Hinrichsen
Technical University of Munich, Catalysis Research Center, Ernst-
Otto-Fischer-Straße 1, 85748 Garching, Germany.

only the duration of the heating step can be shortened, as the cooling step cannot be conducted indirectly. [6, 8]

In contrast, the energy to heat up the adsorbents in an indirect TSA comes from a heat transfer fluid (HTF) that is not in direct contact with the adsorbent material. This indirect heat transfer can be established in a shell and tube heat exchanger adsorber [9] or with structured adsorbents, e.g., hollow fibers [10]. In principle, these indirect TSA methods use two different fluid channels: one for the HTF and one for the process gas. In tube bundle adsorbents, the adsorbent can be inside [9] or outside the tubes [7]. With these setups, mass transfer between those two fluids is prevented; only heat is exchanged. To increase the energy efficiency, the shape of the tubing can be modified, e.g., by fins [7]. As a HTF, oil, water or steam can be used depending on the temperatures required by the process [9].

The main advantage of these new indirect TSA concepts is that little to no regeneration gas is needed to heat and to cool the adsorbent [11]. As a result, the cycle time is independent of the availability of regeneration gas, which allows shorter cycle times [7]. With the indirect heat transfer, not only the heating step, but also the cooling step can be conducted indirectly and thus faster. Furthermore, the released heat of adsorption can be fully removed by continuous cooling during the adsorption step [12]. Consequently, the working capacity of the adsorbent can be improved compared to a conventional TSA process. Most published research on indirect TSAs deals with carbon capture [11–16]. It is shown that this process is able to recover CO₂ with high purity at high recovery rate [13, 14]. Apart from CO₂ removal, the process of an indirectly heated and cooled TSA can also be applied to generate a CO₂-free product stream.

The objective of this work is to establish a quasi-continuous process to remove CO₂ from an N₂/CO₂ mixture. Afterwards, the experimentally determined parameters are used to validate a simulation model of the proposed indirect TSA process.

2 Experimental Setup

The setup of the pilot plant is in accordance with the previously published description of Salazar Duarte and co-workers [13]. The pilot plant consists of two main components: three tube bundle adsorbents combined with a heating and cooling system. The nominal tube length is about 2 m with an inner diameter of approx. 33 mm. The inner diameter is chosen based on previous results

[13]. Each tube is filled with 10 % silica gel (SG) and 90 % molecular sieve 13X (MS). SG is used as a guard layer against traces of water present in the feed gas, as the CO₂ capacity of 13X is drastically decreased in the presence of water [17, 18]. Zeolite 13X is chosen because of its high CO₂ adsorption capacity [19, 20]. The adsorbent characteristics are summarized in Sect. S1 of the Supporting Information (SI). Each adsorber is equipped with several valves to direct the gas routing. These valves are controlled by a process control system, in which the step diagram is implemented. Depending on the process step, the valves are either pressure- or time-controlled. A detailed description of each process step is given in Sect. 3.1.

The heating and cooling system controls the temperature of the tube bundle adsorbents. A synthetic oil is used as heat transfer fluid that covers the required temperature range. Depending on the process step, each adsorber has its own temperature profile. To minimize heat losses, the adsorbents and the HTF pipes are completely insulated. Fig. 1 shows a schematic layout of the pilot plant. To get a clear overview, valves are not shown.

One adsorber is equipped with thermocouples measuring the axial temperature inside the adsorbent bed at the center of the tube. As adsorption is an exothermic process, the adsorption front can be visualized with those thermocouples [12]. Tab. 1 shows the axial position of three representative thermocouples. TC_L10 is located in the bottom of the MS layer, slightly above the SG. TC_L04 and TC_L02 are located near the midpoint and the top of the MS layer, respectively.

The CO₂ content in the feed, product and tail gas is measured with an infra-red online analyzer. The N₂ content is

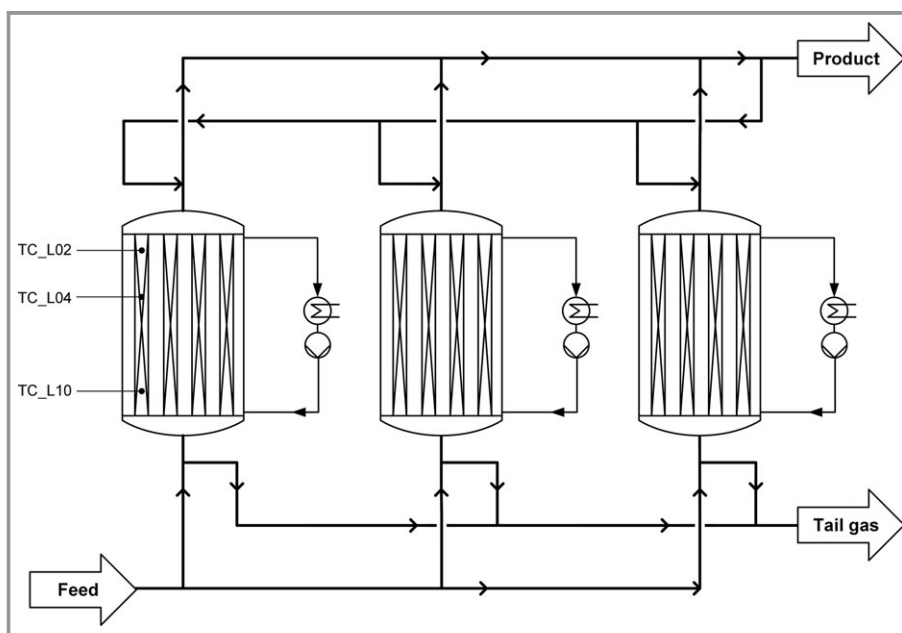


Figure 1. Overview of the pilot plant.

Table 1. Axial positions of the thermocouples in the center of one adsorber tube.

Thermocouple	Axial position
TC_L02	top
TC_L04	middle
TC_L10	bottom

determined solving the mass balance. The gases used for the experiments are summarized in Sect. S2 of the SI.

3 Process Description and Mathematical Model

3.1 Process of an Indirectly Heated and Cooled TSA

Fig. 2 shows the step diagram for a three-adsorber TSA process similar to those suggested by Bonjour et al. [21] and Hosseini et al. [22]. During the adsorption step feed gas is introduced at the bottom of the adsorber via the feed gas inlet valve. The feed contains a mixture of N_2 and CO_2 . CO_2 is removed from the gas stream while the purified product leaves the adsorber on top through the product valve.

During the adsorption step the adsorber is indirectly cooled to remove the released heat of adsorption. This is done to decrease the width of the mass transfer zone (MTZ) and, thus, increase the breakthrough time. As soon as the leading edge of the MTZ reaches the end of the adsorbent bed, the regeneration phase starts. The regeneration is divided into three steps: heating, purging and cooling. During the heating step the adsorbent is indirectly heated up to the desorption temperature level of $200\text{ }^\circ\text{C}$. According to [13, 15], $200\text{ }^\circ\text{C}$ represents a balanced trade-off between energy requirement and working capacity. The pressure rise caused by the increasing temperature is compensated by releasing gas to the tail gas system. After the regeneration temperature is reached, a small part of the purified product is routed through the warm adsorber to purge out the desorbed CO_2 . This purge step further enhances the regeneration by additionally decreasing the CO_2 partial pressure of the gas phase. The desorbed gas together with the purge gas is also sent to the tail gas via the tail gas valve. Afterwards, the adsorber is indirectly cooled down to adsorption temperature level of $35\text{ }^\circ\text{C}$. During the cooling step, purified product is introduced to maintain the pressure level of the

adsorber. Otherwise, the adsorber pressure would significantly drop due to adsorption and contraction of the gas phase. The two other adsorbers run in phase shifts through the same steps in order to establish a quasi-continuous process.

3.2 Mathematical Model

A simulation model is implemented in COMSOL Multiphysics[®] to describe the proposed TSA process with indirect heat transfer. A tube of the tube bundle adsorber is represented by a 2D axial symmetric model that is coupled to a 1D model for the HTF, analogous to the approach published in [13]. Additionally, the dead volume (DV) of the experimental setup is considered. The DV represents the gas volume of the connecting tubing between the adsorber tube and the feed inlet valve or the tail gas outlet valve, respectively. The DV is not insulated and is neither heated nor cooled by the HTF. The DV at the adsorber top can be neglected in general, as it contains almost pure N_2 during the complete cycle and is also not subject to heating and cooling.

The model can be classified into three different sections: 1) adsorbent, adsorpt and gas phase, 2) tube wall, and 3) HTF. Fig. 3 illustrates the model geometry. The corresponding model equations and the boundary conditions are listed in Sect. S3 and S4 of the SI. A detailed description of those equations has been published elsewhere [1, 3, 5, 23, 24].

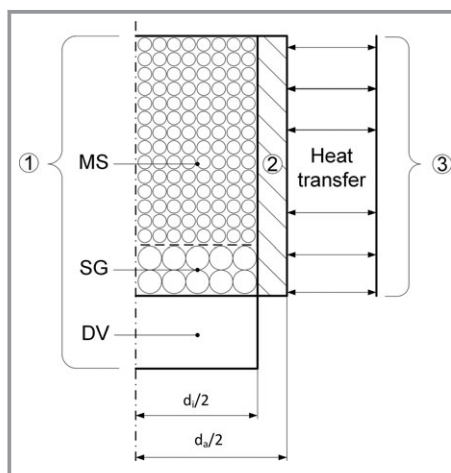
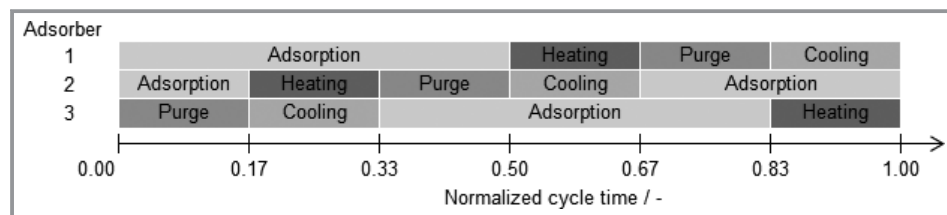


Figure 3. Illustration of the simulation model geometry: 1) molecular sieve (MS), silica gel (SG) and dead volume (DV); 2) tube wall; and 3) heat transfer fluid.

Figure 2. Three adsorber step diagram.



The adsorbent bed can be considered homogeneous and wall effects are neglected, as the d_i/d_p ratio is much larger than 20 [25]. Although the CO₂ isotherm is significantly nonlinear, the linear driving force approach (LDF) is used. According to Sircar and Hufton [26], the LDF model is a justified simplification to describe adsorption kinetics on heterogeneous solids, thus, is appropriate for process simulation. As the Biot number of the mass transfer is much larger than 100, the gas film resistance is negligible compared to the diffusional resistance [27]. Although Hefti et al. as well as Rother et al. [20, 28] show that the ideal adsorbed solution theory (IAST) is not ideal to describe the CO₂-N₂ co-adsorption, especially at high pressures, it represents an acceptable and simplified approach for technical applications [1]. In other published simulation models on indirect TSA, the co-adsorption is usually neglected, as mainly low-pressure applications are investigated. The DV is not insulated and has a high surface area compared to the cross section; therefore, thermal equilibrium with the ambient is expected. All assumptions for the model are summarized below:

- solid and gas phase are in thermal equilibrium,
- homogeneous solid bed with no wall effects,
- SG and MS comprise spherical particles with no particle size distribution,
- gas phase is regarded as ideal,
- kinetics description using the LDF approach,
- film diffusion around adsorbent particles is negligible,
- IAST is used to describe the co-adsorption,
- no pressure drop on the shell side of the adsorber, where HTF flows,
- all tubes of the three adsorbers behave equally, thus, only one tube can be considered,
- the adsorber is perfectly insulated, thus, no heat loss to the surroundings,
- DV is in thermal equilibrium with the surroundings.

3.3 Validation Trends and Indicators

Different trends and performance indicators are compared with the experimental results to validate the simulation model. All experimental data are averaged over two cycles at steady-state operation, which is reached after approx. five cycles from initialization. The simulation is stopped when the loading built up on the adsorbent is deviating cycle over cycle by less than 1%. For the validation, the axial temperature profile and the CO₂ desorption are compared. The CO₂ desorption is described by the CO₂ concentration in the tail gas ($y_{\text{CO}_2, \text{TG}}$) and the tail gas flow (\dot{V}_{TG}). The CO₂ removal rate during the heating and the purge step can be calculated by:

$$V_{\text{CO}_2, \text{step}} = \int_0^{t_{\text{step}}} y_{\text{CO}_2, \text{TG}} \dot{V}_{\text{TG}} dt \quad (1)$$

The required product stream to maintain the adsorber pressure level during the cooling step is evaluated. Additionally, the N₂ recovery is calculated according to Eq. (2), as the focus of this work is on N₂ purification.

$$N_2 \text{ recovery} = \frac{y_{\text{N}_2, \text{Product}} \dot{V}_{\text{Product}}}{y_{\text{N}_2, \text{Feed}} \dot{V}_{\text{Feed}}} \quad (2)$$

4 Validation of the Simulation Model

As adsorption is influenced by temperature, pressure and concentration in addition to the complexity of the theoretical model, different experiments are conducted to validate discrete parts of the model, e.g., the nonconvective heat transfer. Each experiment is conducted at least two times for reproducibility.

4.1 Heat Transfer from the Heat Transfer Fluid to the Outer Tube Wall

The heat conductivity for the adsorbents used in this work and an adjustment factor for the nonconvective heat transfer from the tube wall to the adsorbent are calculated analogous to previous work [29]. Nusselt correlations for tube bundle heat exchangers [24] are implemented to describe the heat transfer from the HTF to the outer tube wall. To cover nonidealities, such as bypasses, and special characteristics of the tube bundle adsorber, an adjustment factor for the heat transfer coefficient is introduced. In order to determine this factor and to validate the simulation model, heating and cooling experiments without convection (closed adsorber in- and outlet) are conducted. Depending on the flow velocity of the HTF through the shell side of the tube bundle adsorber, different heating and cooling times can be realized. As mentioned before, short heating and cooling times are envisaged, thus, the HTF flow was maximized. The adjustment factor was estimated by minimizing the residual sum of squares between the simulated bed temperature and the experimental data. Fig. 4 shows the measured temperature profile in the center of one adsorber tube at TC_L02 in comparison with the simulated values.

The simulated temperature profile in Fig. 4 correlates very closely with the experimental data. The temperature increase as well as the decrease can be described by the simulation model precisely. Only small differences occur in the temperature plateau at 200 °C that can be identified. These differences can be explained by small heat losses from the adsorber occurring in spite of complete insulation. Since the simulation does not include heat losses arising from imperfect insulation, slightly higher temperatures result from the model.

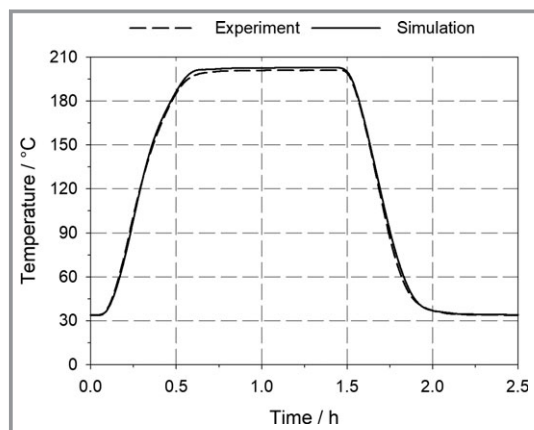


Figure 4. Comparison of the experimental and simulated bed temperature at the adsorber top at the center of the tube for indirect heating and cooling without convection.

4.2 Mass Transfer and Kinetics

Breakthrough experiments are performed to validate the adsorption kinetics and the co-adsorption model. The process conditions for the CO₂ breakthrough measurements are summarized in Tab. 2. Fig. 5 illustrates a comparison of the experimental and the simulated CO₂ concentration at the adsorber outlet and the temperature inside the adsorber tube for this experiment. The adsorbent is indirectly cooled to 35 °C during the whole experiment.

Table 2. Experimental conditions for the CO₂ breakthrough curve.

Parameter	Value
CO ₂ feed content [vol %]	7.6
N ₂ feed content [vol %]	92.4
Pressure [bara]	40
HTF temperature [°C]	35
Feed temperature [°C]	16

Fig. 5a shows a good agreement of the experimental values and the simulated data for the concentration versus time profile. The slope of the CO₂ breakthrough is well reproduced by the simulation model. The slope and the shape of the breakthrough curve represent the adsorption kinetics. The kinetics is described by the LDF approach, which as discussed earlier is a simplified approach. As the simulation results correlate closely with the experiment, the LDF simplification is clearly adequate to describe these adsorption experiments. In Fig. 5b the temperature inside the adsorber tube over time is plotted. The exothermic CO₂ adsorption causes a temperature increase, which is measured with the thermocouples located at the mid-point of the adsorbent bed, at different heights (e.g., top, middle and bottom of the MS layer). As

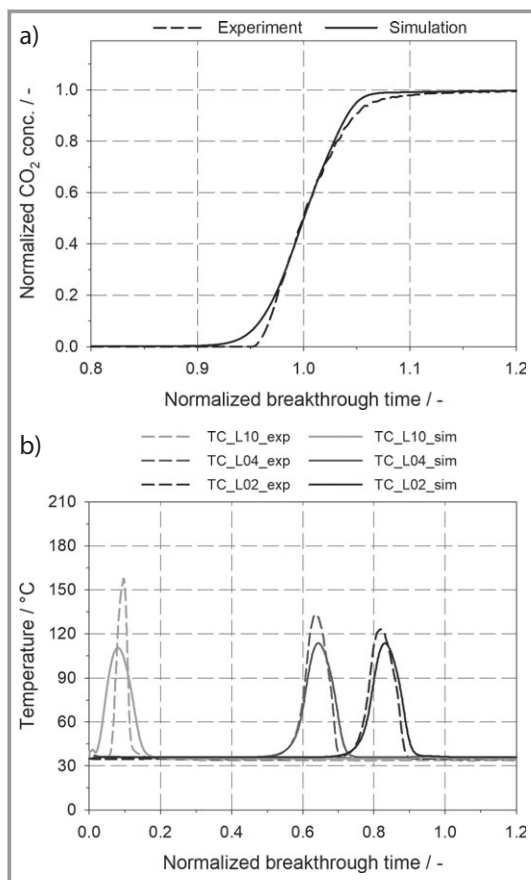


Figure 5. Experimental and simulated values of a) a breakthrough curve with 7.6 vol % CO₂ in N₂ and b) the bed temperature during the breakthrough experiment.

soon as the equilibrium loading is reached, the temperature does not increase any further. During the whole experiment the adsorber is indirectly cooled via the HTF. As a result, the temperature inside the adsorbent bed decreases after the CO₂ adsorption front moves further towards the adsorber outlet. Once more, the good agreement between experiment and simulation shows that the characteristic temperature peaks for this TSA process with indirectly heated and cooled adsorbent can be reproduced.

Analogous to Mulgundmath et al. [12], the exact temperature profile in the molecular sieve layer cannot be described by the simulation. In particular, it is challenging to measure the temperature precisely as the exact axial and especially the radial position is important. As shown in previously published work [29], the radial temperature gradient is very high and, therefore, slight deviations in the exact position of the thermocouples are expected to result in considerable temperature differences, especially when combined with the accuracy of the thermocouples in the experimental system (± 2.5 K). Furthermore, at the bottom of the MS layer, a constant pattern temperature front may not be reached [1], which could be an additional reason for the differences observed. At the adsorber top at TC_L02,

the measured and the simulated temperatures align. In general, the time for each simulated temperature peak corresponds to the experiment. The released heat of adsorption at each position of the thermocouples is compared in Tab. 3. The results of the integrated peak areas of the simulation and the experiment are also similar, within the limit of accuracy of the measurements, as discussed.

Table 3. Relative comparison of the integrated area under each temperature curve during the breakthrough experiment.

Thermocouple	Experiment	Simulation
TC_L02	101.3 ± 6.3	104.2
TC_L04	102.5 ± 6.3	104.3
TC_L10	93.1 ± 6.3	99.9

4.3 Cyclic TSA Process

The sequence for the cyclic TSA process is specified in Sect. 3.1 and the process conditions are summarized in Tab. 4. Fig. 6 shows the axial temperature profile of adsorber 1 measured with the thermocouples located as described in Tab. 1 over one complete cycle.

Table 4. Operating conditions for the cyclic three-adsorber process.

Parameter	Value
CO ₂ feed content [vol %]	4.7
N ₂ feed content [vol %]	95.3
Adsorption pressure [bara]	40.0
Regeneration pressure [bara]	39.8
Adsorption temperature [°C]	35
Desorption temperature [°C]	200
Feed temperature [°C]	16

In the first half of the cycle of Fig. 6, the adsorber is in the adsorption step. The CO₂ adsorption front causes temperature peaks inside the adsorbent bed, analogous to the breakthrough experiment. As already shown in Fig. 5b, the position of the temperature peaks is well described by the simulation, but the absolute height of the peaks differs. From 0.5 to 0.67 of the normalized cycle time, the adsorber is indirectly heated and CO₂ desorption begins. After the adsorber is heated to 200 °C, the purge step takes place until the normalized cycle time of 0.83 is reached. During this purge step, purified product is used to flush the adsorber and to enhance the CO₂ removal by lowering the partial pressure. As a result of the CO₂ desorption, which is endothermic, the temperature decreases. At the bottom of the adsorber at TC_L10, the temperature decrease is lower from

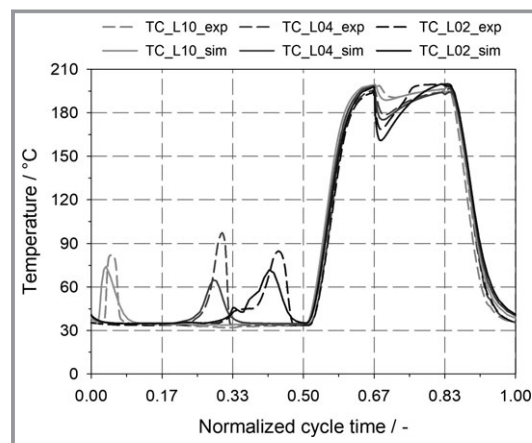


Figure 6. Comparison of the experimental axial temperature profile of adsorber 1 over one complete cycle with the simulated values.

increased CO₂ concentration at the bottom of the adsorption bed. As the desorbing gas leaves the adsorber at the bottom, the CO₂ partial pressure is significantly increased leading to less CO₂ desorption from the bottom layers. This results in a higher residual CO₂ loading at the bottom of the adsorber. The thermocouple TC_L02 shows the highest temperature decrease, as more CO₂ is desorbing, compared to the other positions. After almost complete CO₂ removal at position TC_L02, the temperature rises again to 200 °C. In the following cooling phase from normalized cycle time 0.83 to 1, the adsorber is indirectly cooled back to adsorption temperature.

The CO₂ desorption is further investigated to confirm the theory of the increased CO₂ concentration at the bottom of the adsorbent bed during the purge step. Fig. 7 compares the experimental CO₂ desorption behavior during the heating and purge step with the simulated values. In other published work on this topic, the CO₂ desorption is not investigated in full detail. In order to optimize the process, an in-depth understanding of the desorption is required.

In Fig. 7a, the measured CO₂ concentration and the simulated concentration for cases with and without the DV accounted for is plotted against the normalized cycle time. In Fig. 7a the consideration of the DV becomes significant as the CO₂ concentration profile at the adsorber outlet is different. In the beginning of the heating step, the CO₂ concentration stays at feed level, as the DV is completely filled with feed gas. After the gas volume of the DV is exchanged completely, the CO₂ concentration rises to a certain level. A plateau at the end of the heating step is reached, as the adsorber is almost completely heated and no further desorption or gas expansion occurs. After the introduction of the purge gas at a normalized cycle time of 0.67, a CO₂ concentration peak is flushed out of the adsorber and the DV. Shortly after the purge gas introduction the CO₂ outlet concentration drops significantly due to dilution. At the end of the purge step, the CO₂ concentration is similar at both the

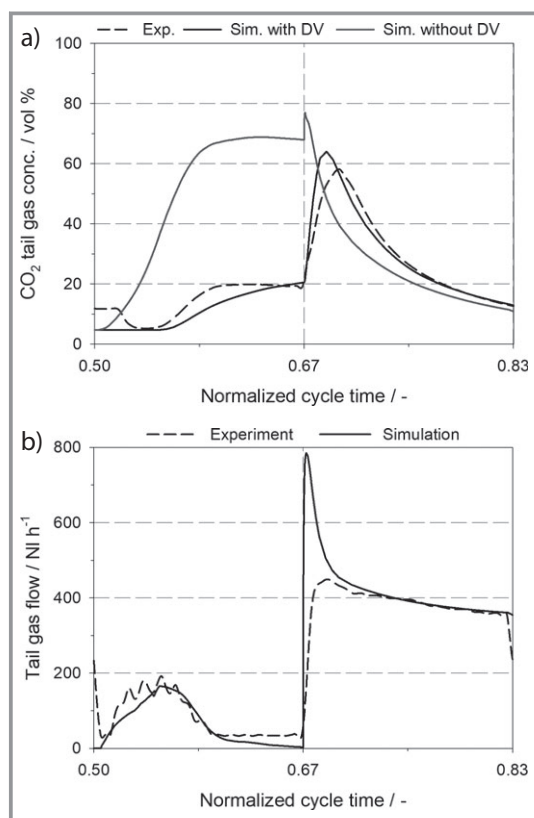


Figure 7. Comparison of the experimental and the simulated a) CO₂ tail gas concentration at the outlet of the adsorber and at the outlet of the dead volume (DV) and b) tail gas flow, during heating and purge step.

adsorber outlet and at the outlet of the DV. In general, the differences during the purge step are far less pronounced, caused by the increased tail gas flow and, hence, the shorter residence time in the DV.

Fig. 7b displays the experimental and the simulated tail gas flow at the outlet of the DV. At the end of the heating step, the simulated tail gas stream diminishes, as the adsorber is completely heated and no more gas is released from the adsorber. The measured tail gas flow does not approach zero, as a small gas flow is continuously sent to the gas analytics and subsequently to the flow meter. As a consequence, a slight pressure drop in the tail gas line can be measured. After the step change from heating to purge at 0.67 of the normalized cycle time, the pressure rises again. As this phenomenon is not considered in the simulation, deviations in the tail gas flow at the end of the heating step and in the beginning of the purge step can be observed. In summary, the DV at the bottom of the adsorber has to be considered to align the experimental and simulated CO₂ desorption behavior.

The required product stream to maintain the adsorption pressure level of the adsorber during the cooling step is plotted in Fig. 8. Due to the much higher adsorption pressure compared to previous published research, the cooling

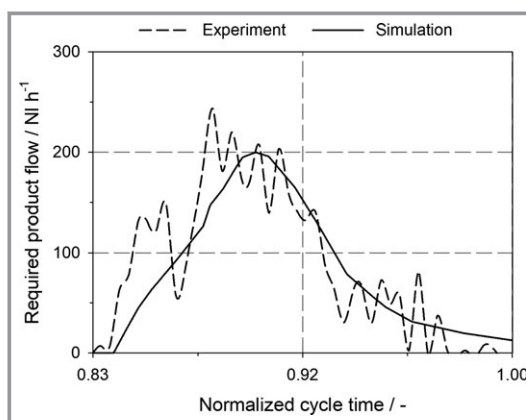


Figure 8. Comparison of the required product flow during the cooling step to maintain the pressure of the adsorber from the experiment and the simulation.

step looks completely different and needs to receive more attention. In particular for the recovery calculation, the amount of product introduced to the adsorber in the cooling step is indispensable.

The fluctuations in the measured flow in Fig. 8 are caused by the switching of the product valve in order to introduce high pressure product. Similar to the tail gas flow at the end of the heating step, the required product at the end of the cooling step approaches zero, as the adsorber is almost cooled down to 35 °C. Taking the measurement accuracy into consideration, the simulation correlates well with the experiment. In comparison to atmospheric pressure applications, the required product flow is much higher.

In Tab. 5 key parameters of the experiment and the simulation are summarized together with the absolute measurement uncertainties. The simulation shows a higher N₂ recovery than the experiment, but within the measurement accuracy. The average CO₂ breakthrough from the simulation is considerably higher than the measured one. The MTZ is very sharp, especially due to the indirect cooling during the adsorption step. As a consequence, slight variations within the measurement accuracy of the CO₂ concentration in the feed gas or the purge gas flow rate result in significant changes in the CO₂ breakthrough. The required

Table 5. Comparison of key parameters.

Parameter	Experiment	Simulation
N ₂ recovery [%]	86.4 ± 0.9	87.2
Average CO ₂ in product [Vppm]	2 ± 5	41
Average CO ₂ in tail gas [vol %]	21.8 ± 1	19.7
N ₂ to maintain pressure during cooling step [NL]	65.2 ± 2.7	61.5
CO ₂ removal during heating step [NL]	6.9 ± 1.5	3.2
CO ₂ removal during purge step [NL]	93.6 ± 4.7	102.4

product during the cooling step to maintain the pressure level lies within the measurement uncertainties. As already discussed at Fig. 7b, the CO₂ removal rates differ between the simulation and the experiment due to a continuous tail gas stream to the analyzer. However, most of the CO₂ is removed during the purge step. Bonjour et al. [21] reiterates the purge gas flow is a critical parameter of such a TSA process, especially in relation to the N₂ recovery rate. Overall, taking all the trends of Figs. 6–8 and the results from Tab. 5 into consideration, the simulation model is validated.

5 Conclusion

A temperature swing adsorption process with indirectly heated and cooled adsorbers for the separation of CO₂ from an N₂/CO₂ mixture is investigated. A quasi-continuous TSA process with three tube bundle adsorbers is established. Additionally, the experimentally determined data are compared with a 2D simulation model set up in COMSOL Multiphysics®. In general, the simulation results correlate well with the experiment.

The proposed simulation model is able to describe non-convective heating and cooling experiments, as well as the CO₂ breakthrough curve. The experimentally determined slope of a breakthrough curve fits together with the concentration values in the simulation. Only the temperature peaks inside the adsorbent bed, caused by the CO₂ adsorption, show slight deviations particularly at the adsorber inlet. Nevertheless, the released heat of adsorption and the timing of the peaks are in good agreement. The adjusted model is used to simulate a cyclic TSA process for the removal of CO₂ from an N₂/CO₂ mixture. Still, the maximum values of the temperature peaks during the adsorption step show slight deviations from the experiment. The simulation reflects well the axial temperature profile. Notably the temperature decrease during the purge step due to desorption corresponds closely with the experiment. During the purge step most CO₂ is removed. However, the adsorbent is not completely regenerated, which becomes apparent in a residual CO₂ loading built up during the first cycles. As a result, multiple cycles are necessary to reach steady state. To describe correctly the experimentally determined CO₂ desorption behavior, the dead volume of the experimental setup is implemented in the simulation model. The dead volume at the adsorber bottom needs to be considered, because of its significant influence on the CO₂ rejection and the N₂ recovery rate.

In summary, the results of the simulation correspond well with the experimental values. The model depicts the adsorption kinetics as well as the CO₂ adsorption and desorption. As a result, the model is validated and can be used for the simulation of an indirect temperature swing adsorption process. Moreover, the experiments show that the proposed TSA process is not only suitable for carbon capture, but also for use in high purity gas stream production.

Supporting Information

Supporting Information for this article can be found under DOI: <https://doi.org/10.1002/cite.201900170>.

Thomas Ried is thankful for the support from TUM Graduate School.

Symbols used

A	[m ²]	surface area
B	[-]	parameter of the model of Zehner/Bauer/Schlünder
b	[bar ⁻¹]	Langmuir parameter
c	[mol m ⁻³]	concentration
c_p	[J kg ⁻¹ K ⁻¹]	specific heat capacity
D	[m ² s ⁻¹]	dispersion/diffusion coefficient
D_i	[m]	adsorber diameter
d	[m]	tube/particle diameter
F	[-]	correction factor
H	[m]	adsorber height
ΔH_{ads}	[J mol ⁻¹]	adsorption enthalpy
K_r	[-]	radial dispersion correction coefficient
$k_{\text{LDF},j}$	[s ⁻¹]	kinetic parameter
M	[kg kmol ⁻¹]	molecular weight
m	[kg]	mass
N	[-]	parameter of the model of Zehner/Bauer/Schlünder
n	[-]	number of tubes of the tube bundle in a row
Nu	[-]	Nusselt number
p	[bar]	pressure
Pr	[-]	Prandtl number
q	[mol kg ⁻¹]	adsorbent loading
q_s	[mol kg ⁻¹]	saturation loading
R	[kJ kmol ⁻¹ K ⁻¹]	ideal gas constant
Re	[-]	Reynolds number
r	[m]	radius
S	[mm]	distance between baffle plates
s_2	[mm]	parameter of the tube bundle
T	[K]	temperature
t	[s]	time
u	[m s ⁻¹]	velocity
u_0	[m s ⁻¹]	superficial velocity
V_D	[m ³]	atomic diffusion volume
\dot{V}_n	[NL h ⁻¹]	standard volume flow at 273.15 K and 1013 mbar
y_j	[-]	volume fraction of component i

Greek symbols

α	[W m ⁻² K ⁻¹]	heat transfer coefficient
ε	[-]	bed porosity

η	[Pa s]	dynamic viscosity
λ	[W m ⁻¹ K ⁻¹]	heat conduction coefficient
ρ	[kg m ⁻³]	density
τ	[-]	tortuosity
ϕ	[m ⁻¹]	surface to volume ratio
Ψ	[-]	free cross-section area of the tube bundle

Sub- and Superscripts

a	outer
Ads	adsorbent
ax	axial
bed	adsorbent bed/filling
Diff	gas diffusion
eff	effective
g	gas phase
i	inner
in	inlet
j	component j
Kn	Knudsen
n	standard condition
p	particle
rad	radial
t	tube
w	wall

Abbreviations

DV	dead volume
exp	experimental value
HTF	heat transfer fluid
IAST	ideal adsorbed solution theory
LDF	linear driving force
MS	molecular sieve
MTZ	mass transfer zone
PSA	pressure swing adsorption
sim	simulated value
SG	silica gel
TG	tail gas
TSA	temperature swing adsorption

References

- [1] W. Kast, *Adsorption aus der Gasphase: Ingenieurwissenschaftliche Grundlagen und technische Verfahren*, VCH, Weinheim **1988**.
- [2] U. von Gemmingen, A. Mersmann, P. Schweighart, *Adsorptionsapparate, Verfahrenstechnische Berechnungsmethoden Teil 2: Thermisches Trennen*, Deutscher Verlag für Grundstoffindustrie, Stuttgart **1996**.
- [3] D. M. Ruthven, *Principles of Adsorption and Adsorption Processes*, John Wiley & Sons, New York **1984**.
- [4] A. Mersmann, M. Kind, J. Stichlmair, *Thermische Verfahrenstechnik, Grundlagen und Methoden*, 2nd ed., Springer-Verlag, Berlin **2005**.
- [5] D. Bathen, M. Breitbach, *Adsorptionstechnik*, Springer-Verlag, Berlin **2001**.
- [6] H. An, B. Feng, S. Su, *Int. J. Greenhouse Gas Control* **2011**, 5 (1), 16–25. DOI: <https://doi.org/10.1016/j.ijggc.2010.03.007>
- [7] J. Bonjour, J.-B. Chalfen, F. Meunier, *Ind. Eng. Chem. Res.* **2002**, 41 (23), 5802–5811. DOI: <https://doi.org/10.1021/ie011011j>
- [8] G. Salazar Duarte, B. Schuerer, C. Voss, D. Bathen, *Chem. Bio. Eng. Rev.* **2017**, 4 (5), 277–288. DOI: <https://doi.org/10.1002/cben.201600029>
- [9] S. Sircar, *US Patent 2003/0037672*, **2003**.
- [10] R. P. Lively, R. R. Chance, W. J. Koros, *Ind. Eng. Chem. Res.* **2010**, 49 (16), 7550–7562. DOI: <https://doi.org/10.1021/ie100806g>
- [11] J. Mérel, M. Clause, F. Meunier, *Environ. Prog.* **2006**, 25 (4), 327–333. DOI: <https://doi.org/10.1002/ep.10166>
- [12] V. P. Mulgundmath, R. A. Jones, F. H. Tezel, J. Thibault, *Sep. Purif. Technol.* **2012**, 85, 17–27. DOI: <https://doi.org/10.1016/j.seppur.2011.07.038>
- [13] G. Salazar Duarte, B. Schuerer, C. Voss, D. Bathen, *Chem. Ing. Tech.* **2016**, 88 (3), 336–345. DOI: <https://doi.org/10.1002/cite.201500031>
- [14] L. Joss, M. Gazzani, M. Mazzotti, *Chem. Eng. Sci.* **2017**, 158, 381–394. DOI: <https://doi.org/10.1016/j.ces.2016.10.013>
- [15] M. Clause, J. Merel, F. Meunier, *Int. J. Greenhouse Gas Control* **2011**, 5, 1206–1213. DOI: <https://doi.org/10.1016/j.ijggc.2011.05.036>
- [16] A. Ntiamoah, J. Ling, P. Xiao, P. A. Webley, Y. Zhai, *Ind. Eng. Chem. Res.* **2016**, 55 (3), 703–713. DOI: <https://doi.org/10.1021/acs.iecr.5b01384>
- [17] F. Brandani, D. M. Ruthven, *Ind. Eng. Chem. Res.* **2004**, 43 (26), 8339–8344. DOI: <https://doi.org/10.1021/ie040183o>
- [18] Y. Wang, M. D. LeVan, *J. Chem. Eng. Data* **2010**, 55 (9), 3189–3195. DOI: <https://doi.org/10.1021/je100053g>
- [19] S. Cavenati, C. A. Grande, A. E. Rodrigues, *J. Chem. Eng. Data* **2004**, 49 (4), 1095–1101. DOI: <https://doi.org/10.1021/je0498917>
- [20] M. Hefti, D. Marx, L. Joss, M. Mazzotti, *Microporous Mesoporous Mat.* **2015**, 215 (6), 215–228. DOI: <https://doi.org/10.1016/j.micromeso.2015.05.044>
- [21] J. Bonjour, M. Clause, F. Meunier, *Chem. Eng. Process.* **2005**, 44 (9), 969–977. DOI: <https://doi.org/10.1016/j.cep.2005.01.002>
- [22] S. F. Hosseini, M. R. Talaie, S. Aghamiri, M. H. Khademi, M. Gholami, M. N. Esfahany, *Sep. Purif. Technol.* **2017**, 183, 181–193. DOI: <https://doi.org/10.1016/j.seppur.2017.03.017>
- [23] R. Bird, W. Stewart, E. Lightfoot, *Transport Phenomena*, 2nd ed., John Wiley & Sons, New York **2002**.
- [24] *VDI-Wärmeatlas*, 11th ed., Springer Verlag, Berlin **2013**.
- [25] W. Kwapinski, M. Winterberg, E. Tsotsas, D. Mewes, *Chem. Eng. Technol.* **2004**, 27 (11), 1179–1186. DOI: <https://doi.org/10.1002/ceat.200407001>
- [26] S. Sircar, J. R. Hufton, *Adsorption* **2000**, 6 (2), 137–147. DOI: <https://doi.org/10.1023/A:1008965317983>
- [27] D. D. Do, *Adsorption Analysis: Equilibria and Kinetics*, 2nd ed., Series on Chemical Engineering, Imperial College Press, London **1998**.
- [28] J. Rother, T. Fieback, *Adsorption* **2013**, 19 (5), 1065–1074. DOI: <https://doi.org/10.1007/s10450-013-9527-2>
- [29] G. Salazar Duarte, *Carbon dioxide removal from industrial gases using an indirectly heated and cooled temperature swing adsorption process*, Ph.D. Thesis, University Duisburg-Essen **2017**.
- [30] M. Nilles, *Wärmeübertragung an der Wand durchströmter Schüttungsrohre*, Ph.D. Thesis, University Karlsruhe **1991**.
- [31] E. N. Fuller, K. Ensley, J. C. Giddings, *J. Phys. Chem.* **1969**, 73 (11), 3679–3685. DOI: <https://doi.org/10.1021/j100845a020>
- [32] S. Ergun, *Chem. Eng. Prog.* **1952**, 48 (2), 89–94.